Absorption and intensity-dependent photoluminescence measurements on CdSe quantum dots: assignment of the first electronic transitions

A. I. Ekimov,* F. Hache, M. C. Schanne-Klein, D. Ricard, and C. Flytzanis

Laboratoire d'Optique Quantique du Centre National de la Recherche Scientifique, Ecole Polytechnique, 91128 Palaiseau Cedex, France

I. A. Kudryavtsev, T. V. Yazeva, and A. V. Rodina

Ioffe Physicotechnical Institute, St. Petersburg 194021, Russia

Al. L. Efros

Fakultät für Physik, Technische Universität München, Physik Department, James-Franck-Strasse, 8096 Garching/München, Germany

Received January 2, 1992; revised manuscript received April 7, 1992

CdSe is used as a prototype to show the implications of valence-band degeneracy for the optical properties of strongly quantum-confined nanocrystals. Absorption spectra and photoluminescence spectra obtained under intermediate and strong pulsed excitation show the presence of new structures. The energy levels for the electron and the hole are calculated with the spherical confinement, the nonparabolicity of the conduction band, and the valence band degeneracy taken into account. The oscillator strengths of the dipole-allowed transitions are also calculated. This model is found to be in good agreement with the experimental observations, which originate mainly from the quantization of the energy spectrum of holes with due account given to valence-band degeneracy.

1. INTRODUCTION

In the past few years there has been a growing interest in confined electronic systems: quantum wells, quantum dots, and, more recently, quantum wires. Quantum dots[1–5] are roughly spherical semiconductor nanocrystals in suspension in various dielectric media, such as alkali halides, liquids, polymer films, and glass. When the mean particle radius $\bar{a}$ is larger than ~3 times the exciton Bohr radius a_{exc}, one is in the weak-confinement regime: the confinement kinetic energy is smaller than the Coulomb interaction energy between the electron and the hole, so that the Wannier exciton still exists and is confined as a whole. When the electron confinement energy and the Coulomb interaction energy are of the same order of magnitude, one has the intermediate-confinement situation. Finally, when $\bar{a}$ is a few times smaller than a_{exc}, one has the strong-confinement situation, in which both carriers are independently confined.

In the case of CuBr and CdS for which a_{exc} is 1.8 and 2.8 nm, respectively, the crystal sizes often correspond to the intermediate-confinement situation. In these cases analytic calculation of the eigenenergies and (envelope) eigenfunctions is not possible. The large difference between the electron and the hole effective masses, however, permits adiabatic separation of their movement[2]: the electron wave function is size quantized, whereas the hole moves in the Coulomb potential caused by the electron and is pushed toward the center of the nanocrystal.[6] A different approach to this problem was developed, in which the results obtained in the strong-confinement regime provide the starting point for the process of diagonalization of the Hamiltonian by either perturbation or variation calculations.[3,7] Image charges resulting from the difference between dielectric constants of the nanocrystal and the embedding medium were also taken into account in both formalisms.[3,6]

However, most of the analysis reported up to now suffers from an oversimplifying hypothesis: Only one valence band is considered. In the strong-confinement regime, for example, the confinement kinetic energy is then $\hbar^2\alpha_{\ell n}^2/(2ma^2)$, where $\alpha_{\ell n}$ is the nth zero of the spherical Bessel function of order ℓ and m is the effective mass of the electron or of the hole. At this point only transitions that conserve n and ℓ are allowed, with an oscillator strength proportional to $(2\ell + 1)$. Inclusion of the Coulomb interaction, for example, does not strongly modify these selection rules. The single-valence-band hypothesis overlooks the fact that the valence band originates from p atomic orbitals and is therefore sixfold degenerate when spin is taken into account. The Hamiltonian for this system in the bulk was written by Luttinger and Kohn,[8] who introduced the three parameters, γ_1, γ_2, and γ_3, plus the spin–orbit coupling Δ. This Hamiltonian leads to three valence bands in the bulk with a small warping proportional to $(\gamma_2 - \gamma_3)$. Neglecting this anisotropy and setting $\gamma = \gamma_2 = \gamma_3$, one obtains a split-off band, a heavy-hole band, and a light-hole band, with the corresponding effec-

0740-3224/93/010100-08$05.00

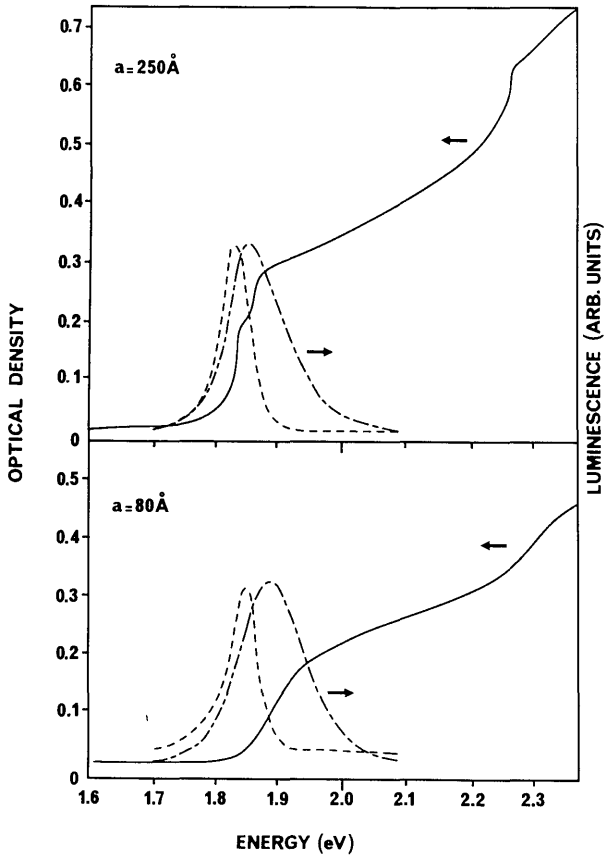

Fig. 1. Absorption spectra (solid curves) and luminescence spectra obtained under weak or intermediate (dashed curves) and strong (short-and-long-dashed curves) excitation at $\lambda = 355$ nm for the samples containing CdSe particles with the largest mean radii, 250 Å (top) and 80 Å (bottom). The luminescence intensity is given in arbitrary units.

tive masses being $m_s = m_0/\gamma_1$, $m_h = m_0/(\gamma_1 - 2\gamma)$, and $m_l = m_0/(\gamma_1 + 2\gamma)$, where m_0 is the free electron mass.

For quantum dots with a spherical confining geometry, this valence-band degeneracy was taken into account in the weak-confinement case for CuCl.[9] Quantum confinement was used to determine the previously unknown band parameters γ_1 and γ. In the strong-confinement case, more recently Efros and Rodina[10] correctly obtained the eigenenergies of the first hole levels in the case $\Delta = 0$ (close to the CdS situation) and in the case $\Delta = \infty$ (also a situation approximately like that for CdSe) in the limit $m_l \ll m_h$, results that were later[11] extended to the case of a finite Δ (the real CdS value) and various values of m_l and m_h. Valence-band degeneracy was also taken into account by Xia.[12] The main point is that the true quantum number is the total angular momentum F. Since the hole wave functions are now linear combinations of wave functions obtained for a single valence band, the selection rules are not so simple as stated above.

CdSe, for which $a_{exc} = 5.6$ nm, is a good candidate for testing the effects of this valence-band degeneracy in the strong-confinement case. We therefore grew CdSe nanocrystals in a glass matrix with various radii, with some of the nanocrystals being smaller than a_{exc}, and studied their optical properties. First we report, in Section 2, experimental results obtained for these CdSe-doped glasses by using absorption spectroscopy and luminescence spectroscopy at medium and high excitation intensity. These spectra reveal the presence of previously unobserved structures. Then we present, in Section 3, results of a complete calculation of the energy levels for CdSe quantum dots, taking into account the spherical confinement, the valence band degeneracy, the nonparabolicity of the conduction band, and the Coulomb interaction between the electron and the hole as well as calculations of the oscillator strengths of the allowed transitions. The experimental results reported in Section 2 are then discussed in Section 4 in the light of these theoretical predictions and are seen to provide experimental support for the predictions: The observed structures originate from the quantization of the energy spectrum of holes.

2. EXPERIMENTS AND RESULTS

A. Absorption Spectra

Samples of CdSe-doped glass were grown by using a zinc-free silicate melt. They were heat treated in the conventional way with a 2-h heat treatment at various temperatures. In the present study five samples are used, for which the mean particle radii $\bar{a}$, as determined by small-angle x-ray scattering are 250, 80, 38, 26, and 21 Å. Their absorption spectra were measured at liquid-nitrogen temperature. The results are shown in Figs. 1 and 2.

The absorption spectrum for the 250-Å sample is the same as for bulk CdSe, with three absorption edges at

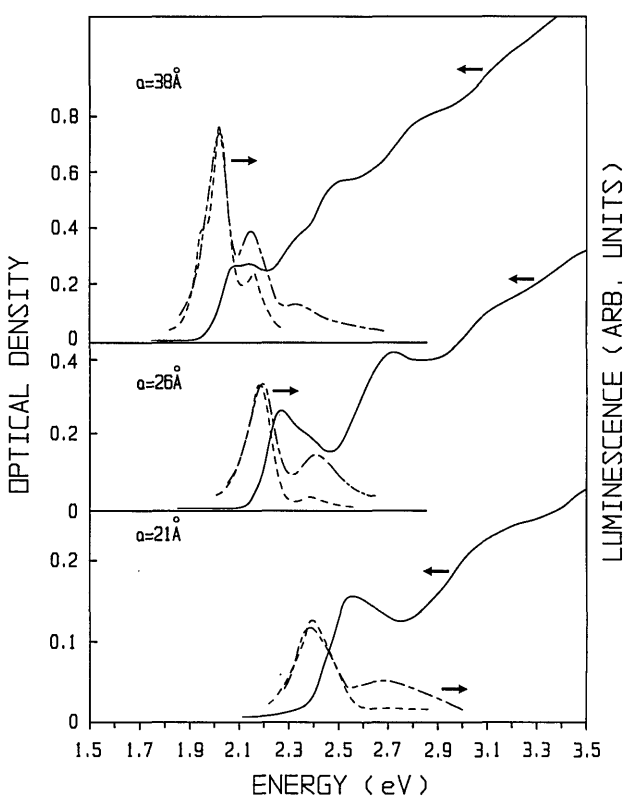

Fig. 2. Absorption spectra (solid curves) and luminescence spectra obtained under weak or intermediate (dashed curves) and strong (short-and-long-dashed curve) excitation at $\lambda = 355$ nm for the samples containing quantum-confined CdSe particles with mean radii of 38 Å (top), 26 Å (middle), and 21 Å (bottom). In the last case the luminescence was weak and the signal-to-noise ratio was low.

~1.84, 1.86, and 2.26 eV, corresponding to the top of the heavy-hole, the light-hole, and the spin–orbit split-off bands, respectively. The absorption spectrum of the 80-Å sample also does not show the structures that are typical of quantum confinement, but, although the split-off band is still clearly visible, the light-hole and the heavy-hole bands seem to have merged into a single edge. For the other three samples, as can be seen in Fig. 2, the quantum size effect clearly shows up, but the first band shows a substructure and, especially for the 38-Å sample, the absorption spectrum shows many more structures than previously observed. For this 38-Å sample the first band shows two peaks that are approximately equally intense at ~2.06 and 2.13 eV. For the 26-Å sample the first peak dominates at ~2.25 eV, while the second one shows up as a shoulder at ~2.38 eV. Finally, for the 21-Å sample only the first peak is visible at ~2.55 eV, with the second one being hidden by other features.

B. Luminescence Spectra

Luminescence spectra were also obtained at liquid-nitrogen temperature with pulsed excitation. The laser pulse derived from a *Q*-switched and mode-locked Nd:YAG laser after frequency doubling ($\lambda = 532$ nm) or frequency tripling ($\lambda = 355$ nm) had a duration of ~25 ps. Luminescence spectra were obtained by using a Jobin–Yvon HRP spectrometer with a 60-cm focal length and a 150-groove/mm grating equipped with a gated optical multichannel analyzer. The 5-ns gate allowed us to record only the fast component of the luminescence and to reject the slow component, especially the broad feature that was due to deep traps. For all five samples excitation at $\lambda = 355$ nm was used; when possible, excitation at $\lambda = 532$ nm was also used but did not lead to different results.

The energy fluence of the laser pulse at the sample could be varied up to ~7 mJ/cm^2. The luminescence spectrum depends on this fluence, as is shown also in Figs. 1 and 2. For each sample two luminescence spectra are shown, one obtained under intermediate-fluence excitation (typically 1 mJ/cm^2), the other one under high-fluence excitation (typically 5 mJ/cm^2). Since the absorbance of the 0.5-mm thick samples was weak, typically 0.3 at the top of the first absorption band, luminescence spectra were not corrected for reabsorption.

For the largest particles, 250 and 80 Å, intermediate-energy excitation leads to band-edge luminescence at ~1.83 and 1.85 eV, respectively. Increasing the excitation energy fluence leads to a blue shift and a broadening of the luminescence peak as shown in Fig. 1, a feature that is typical of band filling. As can be seen in Fig. 2, for the quantum-confined sizes 38, 26, and 21 Å, hot luminescence is also observed but is qualitatively different. New peaks appear instead of the previous shift and broadening. At low and intermediate excitation energies one peak is observed near the absorption edge at 2.00, 2.16, and 2.38 eV, but we observe that the Stokes shift between this peak and the first absorption peak increases when the particle size decreases, as was previously observed.[13] At higher excitation energies a new hot luminescence peak appears; its spectral position coincides wih that of the second absorption peak discussed above. For the 38-Å sample under high excitation, as can be seen from Fig. 2, a second hot peak also appears at ~2.32 eV, also corresponding to one of the absorption features.

It should be emphasized that care was exercised to avoid photodarkening of the samples and that the excitation fluence dependence of the luminescence reported here is fully reversible. These new substructures in the absorption spectrum and hot luminescence peaks, characteristic of state filling, cannot be explained by the conventional formalism that assumes a single valence band. In Section 3 a model that takes valence-band degeneracy into account in the strong-confinement case is developed.

3. THEORY

The absorption spectra of nanocrystals are determined by the energy spectrum of electron–hole pairs. In nanocrystals with radii a smaller than the bulk exciton Bohr radius a_{exc}, these spectra are described by the transitions between quantum size levels (QSL's) of holes and electrons. Coulomb electron–hole interaction only shifts to the red the energies of these transitions.

The energy spectrum of these transitions was calculated in the simple parabolic approximation.[2] However, for real semiconductor nanocrystals this approximation does not work. First, the shift of the electron QSL's from the bottom of the conduction band is so large that nonparabolicity of the conduction band and leakage of the electron wave function into the barrier could lead to deviations from the energy levels that are given by simple parabolic band theory. Second, the valence band of semiconductors with cubic and hexagonal lattice structures has a rather complicated many-band structure. As a result, the wave functions of electrons and holes have the following form:

$$\Psi_{e,h} = \sum_{\mu=-1/2}^{1/2} f_{c,\mu}(\mathbf{r}) u_{c,\mu} + \sum_{\mu=-3/2}^{3/2} f_{3/2,\mu}(\mathbf{r}) u_{3/2,\mu} + \sum_{\mu=-1/2}^{1/2} f_{s,\mu}(\mathbf{r}) u_{s,\mu}, \tag{1}$$

where $u_{c,\mu}$, $u_{3/2,\mu}$, and $u_{s,\mu}$ are the Bloch functions of the conduction band and the fourfold degenerate and spin–orbit split-off valence bands and $f_{c,\mu}$, $f_{3/2,\mu}$, and $f_{s,\mu}$ are their corresponding envelope functions.

A. Electron Energy Spectrum

The spectrum of electron QSL's with the nonparabolicity of the conduction band and the finite depth of the quantum well taken into account, was analytically obtained in the many-band approximation for a semiconductor with a vanishing spin–orbit coupling Δ.[14] For $\Delta \neq 0$, similar considerations give the following determination for the QSL's:

$$\frac{E + (E_g^{\,s}/2) + (2\Delta/3)}{E + (E_g^{\,s}/2) + \Delta} \frac{\partial}{\partial r} \ln[j_\ell(\kappa_s r)]|_{r=a} = \frac{E + E_g^{\,s}/2}{E + E_g^{\,g}/2} \frac{\partial}{\partial r} \ln[K_\ell'(\kappa_g r)]|_{r=a} \frac{E + (E_g^{\,g}/2) + (2\Delta/3)}{E + (E_g^{\,g}/2) + \Delta}, \tag{2}$$

where $E_g^{\,s}$ and $E_g^{\,g}$ are the energy gaps of the semiconductor and the glass, E is the energy of the state measured

from the middle of the gap E_g, $j_\ell(z)$ is the spherical Bessel function of order ℓ, and K_ℓ' is connected to the modified Bessel function $K_{\ell+1/2}$ by the relations

$$K_\ell'(z) = (\pi/2z)^{1/2}K_{\ell+1/2}(z),$$

$$\kappa_g^2 = \frac{1}{\hbar^2|V|^2}[(E_g^g/2)^2 - E^2]\frac{E + (E_g^g/2) + \Delta}{E + (E_g^g/2) + (2\Delta/3)},$$

$$\kappa_s^2 = \frac{1}{\hbar^2|V|^2}[E^2 - (E_g^s/2)^2]\frac{E + (E_g^s/2) + \Delta}{E + (E_g^s/2) + (2\Delta/3)}, \quad (3)$$

where $V = \langle S|\hat{p}_z|Z\rangle/m_0$ is the Kane matrix element. Detailed consideration shows that the electron QSL's with $\ell > 1$ are split by the spin–orbit interaction.

Analysis of Eq. (2) shows that it reduces to the simple well-known expression[2]

$$j_\ell(\kappa_s a) = 0 \quad (4)$$

when $\kappa_g a \gg 1$. This result means that the electron component of the envelope function f_c vanishes at the surface of the nanocrystal for deep enough quantum wells, as happens with the electron wave function in the one-band parabolic model.

A contribution of higher bands is necessarily included in the electron effective mass in such wide-gap semiconductors as CdSe. In this case the Schrödinger equation for the electron component of wave function f_c has the following form [see, for comparison, Eq. (6) of Ref. 14]:

$$\left\{1 + 2f + \frac{E_p}{3}\left[\frac{2}{E + E_g/2} + \frac{1}{E + (E_g/2) + \Delta}\right]\right\}\frac{\hat{p}^2}{2m_0}f_c(\mathbf{r}) = \left(E - \frac{E_g}{2}\right)f_c(\mathbf{r}), \quad (5)$$

where the energetic band parameter $E_p = 2V^2m_0$, $2f$ is the contribution of higher bands to the electron effective mass[15] and $\hat{p} = -i\hbar\nabla$ is the momentum operator. The effective electron mass m_e at the bottom of the conduction band ($E = E_g/2$) satisfies the well-known relationship[15]

$$\frac{1}{m_e} = \frac{1}{m_0}\left[1 + 2f + \frac{E_p}{3}\left(\frac{2}{E_g} + \frac{1}{E_g + \Delta}\right)\right]. \quad (6)$$

The solutions of Eq. (5) are the same as in the simple parabolic band approximation:

$$f_c(\mathbf{r}) = A_{\ell k}Y_\ell^m(\theta,\phi)j_\ell(\alpha_{\ell k}r/a) \quad (7)$$

where $Y_\ell^m(\theta,\phi)$ are the spherical harmonics, $A_{\ell k}$ is the normalization constant, and boundary condition (4) determines the value of the numbers $\alpha_{\ell,k}$, which are the zeros of the spherical Bessel functions (the four smallest ones are $\alpha_{0,1} = \pi$, $\alpha_{1,1} \approx 4.49$, $\alpha_{2,1} \approx 5.76$, and $\alpha_{0,2} = 2\pi$). Substituting Eq. (7) into Eq. (5), we obtain the equation that determines the energy $E_{\ell,k} = E - E_g/2$ of electron QSL's:

$$E_{\ell,k} = \left[1 + 2f + \frac{E_p}{3}\left(\frac{2}{E_{\ell,k} + E_g} + \frac{1}{E_{\ell,k} + E_g + \Delta}\right)\right]\frac{\hbar^2\alpha_{\ell,k}^2}{2m_0a^2}. \quad (8)$$

The size dependence of these QSL's energies is presented in Fig. 3.

B. Hole Energy Spectrum

We consider the hole QSL's in the framework of the six-band model, neglecting the electron component f_c in wave function (1). The effective Hamiltonian of this model has the following form in the spherical approximation:

$$\hat{H} = \frac{1}{m_0}\begin{bmatrix} P+Q & L & M & 0 & i\sqrt{1/2}L & -i\sqrt{2}M \\ L^* & P-Q & 0 & M & -i\sqrt{2}Q & i\sqrt{3/2}L \\ M^* & 0 & P-Q & -L & -i\sqrt{3/2}L^* & -i\sqrt{2}Q \\ 0 & M^* & -L^* & P+Q & -i\sqrt{2}M^* & -i\sqrt{1/2}L^* \\ -i\sqrt{1/2}L^* & i\sqrt{2}Q & i\sqrt{3/2}L & i\sqrt{2}M & P-\Delta & 0 \\ i\sqrt{2}M^* & -i\sqrt{3/2}L^* & i\sqrt{2}Q & i\sqrt{1/2}L & 0 & P-\Delta \end{bmatrix}, \quad (9)$$

where

$$P = (\gamma_1/2)\hat{p}^2, \qquad Q = \gamma(\hat{p}_\perp^2 - 2\hat{p}_z^2)/2,$$

$$L = -i\sqrt{3}\gamma\hat{p}_-\hat{p}_z,$$

$$M = \sqrt{3}\gamma\hat{p}_-^2/2, \qquad \hat{p}_\perp^2 = \hat{p}_x^2 + \hat{p}_y^2, \qquad \hat{p}_\mp = \hat{p}_x \mp i\hat{p}_y,$$

$$\hat{p}_x = -i\hbar\frac{\partial}{\partial x}, \qquad \hat{p}_y = -i\hbar\frac{\partial}{\partial y}, \qquad \hat{p}_z = -i\hbar\frac{\partial}{\partial z}.$$

In a spherical potential the hole states are characterized by the total angular momentum $\hat{\mathbf{F}} = \hat{\mathbf{L}} + \hat{\mathbf{J}} + \hat{\mathbf{S}}$, where $\hat{\mathbf{L}}$ is the orbital angular momentum operator for the envelope wave function, $\hat{J}_x$, $\hat{J}_y$, and $\hat{J}_z$ are the 3×3 orbital momentum spin matrices, with $j = 1$ (for the atomic orbitals), and $\hat{\mathbf{S}}$ is the spin 1/2 operator. The states with a given value of the total momentum F are degenerate with respect to the momentum projection M. The parity operator $\hat{I}$ also commutes with the Hamiltonian, Eq. (9). As a result the wave functions of the even states Ψ_{FM}^+ contain the spherical functions Y_ℓ^m with orbital momentum $\ell = F - 3/2$, $\ell = F + 1/2$ and for odd states Ψ_{FM}^- have $\ell = F - 1/2$, $\ell = F + 3/2$ (Refs. 11 and 16):

$$\Psi_{FM}^\pm(\mathbf{r}_h) = \sqrt{2F+1}\left[\sum_{\substack{\ell=F+1/2,\,F-3/2 \\ \ell=F+3/2,\,F-1/2}}(-1)^{\ell-3/2+M}R_\ell^\pm(r_h) \times \sum_{\mu=-3/2}^{3/2}\begin{pmatrix}\ell & 3/2 & F \\ m & \mu & -M\end{pmatrix}Y_\ell^m(\mathbf{r}_h/r_h)u_{3/2,\mu} + (-1)^{F\pm(1/2)-(1/2)+M}R_s^\pm(r_h) \times \sum_{\mu=-1/2}^{1/2}\begin{pmatrix}F\pm1/2 & 1/2 & F \\ m & \mu & -M\end{pmatrix}Y_{F\pm1/2}^m(\mathbf{r}_h/r_h)u_{s,\mu}\right], \quad (10)$$

where $\mathbf{r}_h$ is the hole position in a nanocrystal, and

$$\begin{pmatrix} a & b & c \\ d & e & f \end{pmatrix}$$

are $3j$ Wigner symbols. The radial functions $R_\ell^{\pm}(r)$ and $R_s^{\pm}(r)$ in the spherical nanocrystals can be generally represented as the sum of three spherical Bessel functions $j_\ell(k_t r)$ $(t = l, h, s)$.[11] The arguments correspond to three dependences of the modulus of the wave vectors k_l, k_h, and k_s on the energy eigenvalue E (three branches in the dispersion law for the valence band):

$$k_{l,s}^2 = \frac{m_0}{\hbar^2(\gamma_1 - 2\gamma)(\gamma_1 + 4\gamma)}\{2E(\gamma_1 + \gamma) - \Delta(\gamma_1 + 2\gamma) \pm \{[2E(\gamma_1 + \gamma) - \Delta(\gamma_1 + 2\gamma)]^2 - 4E(E - \Delta)(\gamma_1 - 2\gamma)(\gamma_1 + 4\gamma)\}^{1/2}\},$$

$$k_h^2 = \frac{2m_0 E}{\hbar^2(\gamma_1 - 2\gamma)}. \tag{11}$$

The requirement that the radial functions vanish at the nanocrystal's surface, which corresponds to an infinitely high potential barrier at the semiconductor–glass interface, leads to the dispersion equations for the QSL's. The equation for the odd states takes the form[11]

$$(2F - 1)2\epsilon^-(1/k_s^2 - 1/k_l^2)j_{F-1/2}(k_l a)j_{F+3/2}(k_h a)j_{F-1/2}(k_s a) + 3(2F + 3)\left[\frac{(\gamma_1 + 2\gamma)k_l^2 - 2\epsilon^-}{k_l^2} \times j_{F+3/2}(k_s a)j_{F-1/2}(k_l a)j_{F-1/2}(k_h a) - \frac{(\gamma_1 + 2\gamma)k_s^2 - 2\epsilon^-}{k_s^2} j_{F+3/2}(k_l a)j_{F-1/2}(k_s a)j_{F-1/2}(k_h a)\right] = 0, \tag{12}$$

where $F = 1/2, 3/2, \ldots$, and we introduce the parameters $\epsilon = m_0 E/\hbar^2$ and $\delta = m_0\Delta/\hbar^2$. For the even states we find that

$$(2F + 3)2\epsilon^+(1/k_s^2 - 1/k_l^2)j_{F+1/2}(k_l a)j_{F-3/2}(k_h a)j_{F+1/2}(k_s a) - 3(2F - 1)\left[\frac{(\gamma_1 + 2\gamma)k_s^2 - 2\epsilon^+}{k_s^2} \times j_{F+1/2}(k_s a)j_{F-3/2}(k_l a)j_{F+1/2}(k_h a) - \frac{(\gamma_1 + 2\gamma)k_l^2 - 2\epsilon^+}{k_l^2} j_{F+1/2}(k_l a)j_{F-3/2}(k_s a)j_{F+1/2}(k_h a)\right] = 0, \tag{13}$$

where $F = 3/2, 5/2, \ldots$. If $F = 1/2$, the dispersion equation takes the form

$$j_1(k_l a)j_1(k_s a) = 0. \tag{14}$$

For $\epsilon < \delta$, when $k_s^2 < 0$, the spherical Bessel functions should be considered to be functions of complex argument.

Below, for all these states we use the following notation: for nQ_F, F is the total momentum of state, $Q(S, P, D, F, \ldots)$ is the minimum orbital momentum ℓ included in the hole wave function (the other one is $\ell + 2$), and n is the corresponding number of the level of given symmetry. For example, the ground state of the hole (the even state with $F = 3/2$) includes the orbital momenta $\ell = 0$ and $\ell = 2$ and is denoted $1S_{3/2}$. However, for even states with $F = 1/2$ we must introduce a special notation $nP_{1/2}^{l}$ for QSL's of light holes and $nP_{1/2}^{so}$ for QSL's of holes in the spin–orbit split off band.

The energy dependence of the lowest hole QSL's on the radius of CdSe microcrystals is shown in Fig. 3. All these levels go to the top of the valence band when the nanocrystal size increases. There is only one exception: the levels of $nP_{1/2}^{so}$ states go to the top of the spin–orbit split-off band.

C. Absorption Spectra

As is mentioned above, the structures of absorption spectra are determined by the transitions between QSL's of electrons and holes. The probability of dipole-allowed transitions in semiconductor nanocrystals is determined by the square of the overlap integral between the electron and the hole wave functions[2,10,11]:

$$K = \left|\int \Psi_{k,\ell,m}(\mathbf{r})\Psi_{n,F,M}^{p}(\mathbf{r})\mathrm{d}^3 r\right|^2, \tag{15}$$

where $\Psi_{k,\ell,m}$ are the electron wave functions[2] and $\Psi_{n,F,M}^{p}$ are the hole wave functions determined by Eq. (10). Us-

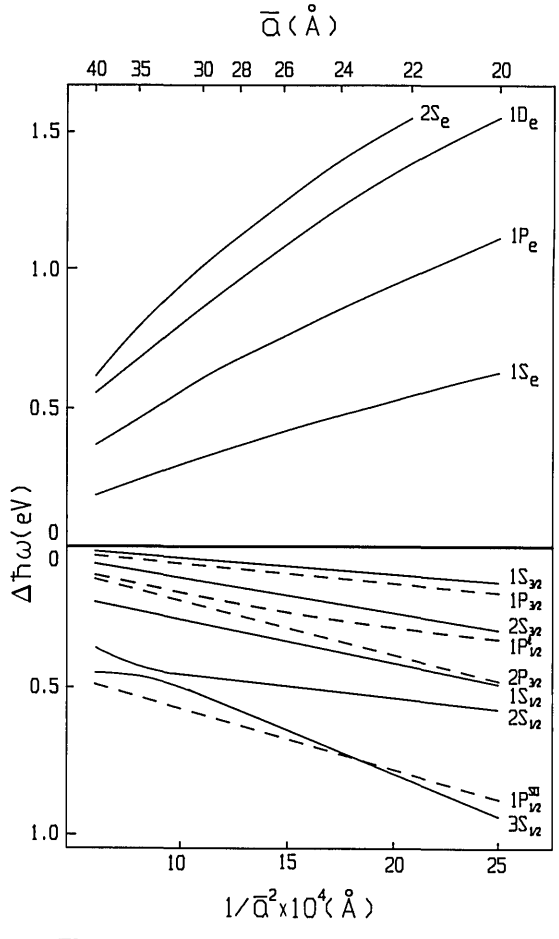

Fig. 3. Electron and hole energy spectra as calculated in Subsection 3.A, plotted versus the inverse-mean-square radius. The electron energy, which increases upward, is referred to the bottom of the conduction band; the hole energy, increasing downward is referred to the top of the valence band. Only those levels involved in transitions with a significant oscillator strength are shown. The P states of the hole are shown as dashed curves.

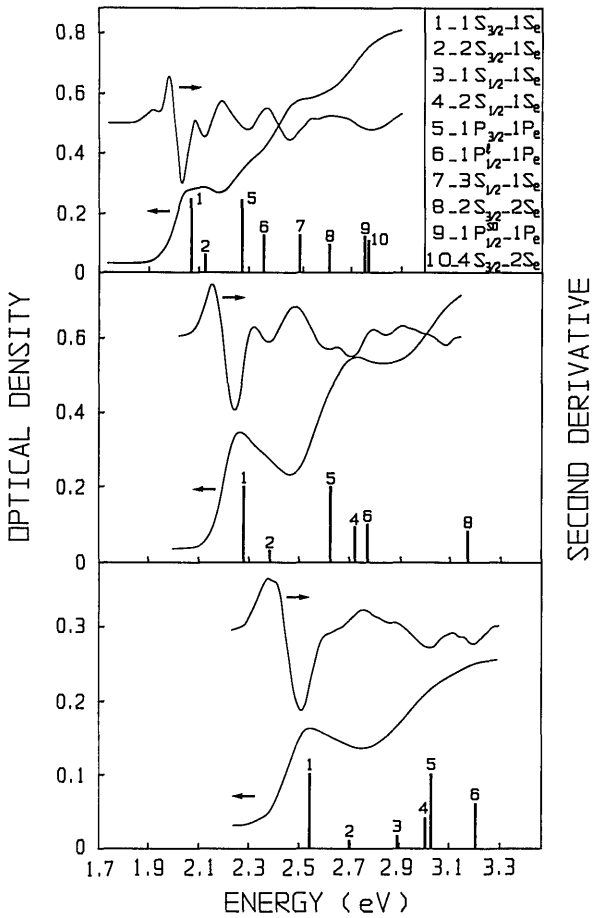

Fig. 4. Comparison between theory and experiment. The absorption spectra shown in Fig. 2 are reproduced with the second-derivative spectra. The calculated positions of the transitions are shown as vertical bars whose height indicates the relative strength (the first or $1S_{3/2}$–$1S_e$ transition is given the same arbitrary height for all three samples). Only the transitions with a significant oscillator strength are shown. The inset shows the assignment of these transitions.

ing only the angular dependence of these wave functions, one can obtain the selection rules for the interband transitions.[11] The transitions to the $1S_e$ and $2S_e$ electron levels are possible from the $nS_{3/2}$ and $nS_{1/2}$ hole QSL's because only wave functions of these hole states involve the spherical harmonic Y_0^0. Similar considerations show that transitions to the $1P_e$ electron level are possible from the $nP_{3/2}$, $nP_{1/2}{}^{l}$, $nP_{1/2}{}^{so}$, and $nP_{5/2}$ hole states and to the $1D_e$ level from the $nS_{3/2}$, $nS_{1/2}$, $nD_{7/2}$, and $nD_{5/2}$ states. Transitions from hole QSL's to electron QSL's with $n \neq k$ are also possible, unlike in the simple parabolic band approximation,[2] and their relative intensity is determined by Eq. (15). Only the transitions $nP_{1/2}{}^{l} \Rightarrow kP_e$ and $nP_{1/2}{}^{so} \Rightarrow kP_e$ are exceptions, because their probabilities at $n \neq k$ are low and are not equal to zero only because of the nonparabolicity of the conduction band and the weak leakage of the electron and the hole wave functions through the barrier.

We can build the absorption spectrum in small nanocrystals, since we know the selection rules and the energy of optical transitions $\hbar\omega$ between the QSL's of holes and electrons. The energy is decreased by the Coulomb electron–hole interaction energy E_{eh}. Correlation of electron and hole motion resulting from the Coulomb potential also leads to splitting of the degenerate QSL's. Neglecting these Coulomb corrections, we can write the energy of transitions as

$$\hbar\omega = E_g + E_{\ell,k} + E^{\pm}(n,F) - E_{eh}, \tag{16}$$

where $E^{\pm}(n,F)$ are the energies of the hole QSL's connected with the roots of Eqs. (12)–(14) by the relationship $E^{\pm}(n,F) = \hbar^2\epsilon^{\pm}(n,F)/m_0$. Below we assume that $E_{eh} = 1.8e^2/\kappa a$ for transitions to the $1S_e$ level and $E_{eh} = 1.7e^2/\kappa a$ for transitions to the $1P_e$ and $1D_e$ levels,[10,17] where κ is the dielectric constant of CdSe.

The positions of the allowed transitions between the hole and the electron QSL's, calculated in accordance with Eq. (16), and their relative intensities, are shown in Fig. 4 by the vertical bars for nanocrystals with mean radii $\bar{a}$ of 21, 26, and 38 Å. Relative intensities for some transitions depend strongly on nanocrystal size. That is why transition 3 in Fig. 4, for instance, should appear only in the spectrum of nanocrystals with a radius of 21 Å. It is seen that the spectral positions of transitions, as well as their relative intensities, are in rather good agreement with the experimental data. The best fit was obtained for the following set of energy-band parameters: $\gamma_1 = 2.1$, $\gamma = 0.55$, $E_p = 17.5$ eV, $E_g = 1.84$ eV, $\Delta = 0.42$ eV, and $f = -0.42$. For several of these parameters we use the known values. Regarding the electron energy levels, for m_e at the bottom of the conduction band our set of parameters gives the value $m_e = 0.11m_0$, in good agreement with the value obtained by Hermann and Weisbuch.[18] However, our combination of E_p and f that gives this value [see Eq. (6)] differs from theirs: $E_p = 18.1$ eV, $f = -0.71$. Our measurements should be more sensitive to the value of E_p, since the optical transitions go deeper into the conduction band than in other experiments. We therefore believe that our parameters E_p and f are more accurate.

4. DISCUSSION

The experimental results that we reported in Section 2 can be understood in terms of the theoretical calculations. The largest two samples, of 250- and 80-Å mean radius, do not show, as expected, strong evidence of quantum confinement of the carriers. This is especially true of the 250-Å sample, which shows the same absorption spectrum and the same band-edge luminescence under weak excitation as does bulk CdSe. This is less clearly true of the 80-Å sample: in its case, the upper two valence bands have merged into one absorption edge, and the band-edge luminescence observed under weak excitation shows a small blue shift. This shift is due to a small quantum size effect (the mean radius $\bar{a}$ is not much larger than a_{exc}), but the confinement effect is too weak to modify the joint density of states strongly, so that the blue shift and the broadening of the luminescence spectra under high-energy excitation observed for these two samples is due to band filling. From the absorbed energy in the strong excitation case we conclude that the photogenerated carrier gas is highly degenerate (the density of excited carriers is of the order of 10^{20} cm^{-3}) and the electron Fermi energy is large enough to account for the shift and the broadening of the luminescence peak that we observe, even assuming

the carrier recombination time to be reduced by a factor of 10.

The situation is radically different for the other three samples, which clearly show the quantum-confinement effect: blue-shifted and structured absorption spectra. This effect is clearly visible in the absorption spectra shown in Fig. 2. Figure 4 shows the second derivative of these absorption spectra together with the positions and intensities of the first allowed transitions as calculated in Section 3. Good agreement is obtained for the positions of the peaks. We assign the first two absorption peaks to the $1S_{3/2}$–$1S_e$ and $2S_{3/2}$–$1S_e$ transitions. (Xia's calculation[12] for ZnSe also showed the second excited state to be $2S_{3/2}$–$1S_e$ with approximately the same relative oscillator strength as here.) The difference in energy between these two transitions increases, whereas the relative oscillator strength of the second decreases, when the size is reduced. The size dependence of the first absorption band is thus well explained.

The third absorption feature for our 38-Å sample may correspond to the $1P_{3/2}$–$1P_e$ transition, to the $1P_{1/2}$–$1P_e$ one, or to a combination of the two. The two hot luminescence peaks observed for this 38-Å sample seem to correspond to the second and the third absorption peaks. In the same way, the hot luminescence peaks that we observe for the 26- and 21-Å samples seem to correspond to the second (the $2S_{3/2}$–$1S_e$) absorption peak. In the case of the 21-Å sample this second absorption peak is not seen experimentally, but the calculated position (2.7 eV) is in good agreement with the luminescence spectrum. For these two samples (26- and 21-Å mean radius) the third absorption peak may be assigned to the $1P_{3/2}$–$1P_e$, the $2S_{1/2}$–$1S_e$, and the $1P_{1/2}$–$1P_e$ transitions. Note that the relative positions of these transitions change with sample size and that they are unresolved in the experimental spectra.

Somewhat similar CdSe absorption spectra were reported previously[19–21] but were not properly assigned. We emphasize that our experimental observations, especially the substructures of the absorption spectrum and the hot luminescence peaks, could not be understood without taking the valence-band degeneracy into account and that the proper way of taking it into account is the one presented in Section 3. Our samples show these previously unobserved rich substructures probably because they have a narrower size distribution: working at low temperature, we strongly reduce the intrinsic broadening, and the remaining width of the absorption peaks is probably due to the size distribution of the nanocrystals, which must be rather small here to permit observation of the substructures that we see.

A few points, however, remain unexplained. First, the Stokes shift between the weak excitation luminescence peak and the first absorption peak, which is observed to increase when the particle size is reduced, is difficult to explain by electron–phonon coupling: It would imply too large a Huang–Rhys S parameter.[22] In Ref. 23 some of us interpreted this luminescence peak in terms of intrinsic surface states. Such surface states cannot be accounted for by the model used in Section 3. Second, at present we do not clearly understand why the hot luminescence peaks in the 38-, 26-, and 21-Å samples correspond to the second and the third absorption peaks and why we do not see any hot luminescence originating from the first excited level (the $1S_{3/2}$–$1S_e$ transition), which theoretically has a larger oscillator strength. This absence could be due to a shorter lifetime or to faster trapping. Time-resolved luminescence and nonlinear absorption measurements now under way may give the answer to this question.

5. CONCLUSION

We have shown in this paper how the valence-band degeneracy gives rise, in the case of CdSe nanocrystals, to substructures in the absorption and luminescence spectra. These new features could be observed because we had better-quality samples. We also showed how to take this valence-band degeneracy into account theoretically; because of coupling between the angular momenta of the atomic wave functions and the envelope wave functions, the true wave functions are eigenfunctions of the total angular momentum F. The corresponding energy eigenvalues and the oscillator strengths of the allowed transitions have also been calculated, and good agreement between theory and experiment has been obtained. This work provides the basis for a better understanding of the linear and the nonlinear optical properties of such II–VI nanocrystals.

This valence-band degeneracy completely modifies the selection rules that were previously thought to prevail, as was also shown by Xia[12]: It was previously shown how this modification explains coupling between carriers and surface phonons[24]; it would also be worth looking at the implications for nonlinear optical properties.

ACKNOWLEDGMENTS

The authors thank C. Hermann for fruitful discussions. Al. L. Efros acknowledges the support of the Deutsche Forschungsgemeinschaft.

*Permanent address, Ioffe Physicotechnical Institute, St. Petersburg 194021, Russia.

REFERENCES

1. A. I. Ekimov and A. A. Onushchenko, JETP Lett. **34,** 345 (1981); **40,** 1137 (1984).
2. Al. L. Efros and A. L. Efros, Sov. Phys. Semicond. **16,** 772 (1982).
3. L. E. Brus, J. Chem. Phys. **80,** 4403 (1984).
4. R. Rossetti, R. Hull, J. M. Gibson and L. E. Brus, J. Chem. Phys. **82,** 552 (1985).
5. H. Weller, H. M. Schmidt, U. Koch, A. Fojtik, S. Baral, A. Henglein, W. Kunath, K. Weiss, and E. Dieman, Chem. Phys. Lett. **124,** 557 (1986).
6. A. I. Ekimov, Al. L. Efros, M. G. Ivanov, A. A. Onushchenko, and S. K. Shumilov, Solid State Commun. **69,** 565 (1989).
7. Y. Z. Hu, M. Lindberg, and S. W. Koch, Phys. Rev. B **42,** 1713 (1990).
8. J. M. Luttinger and W. Kohn, Phys. Rev. **97,** 869 (1955); J. M. Luttinger, Phys. Rev. **102,** 1030 (1956); see also N. O. Lipari and A. Baldereschi, Phys. Rev. Lett. **25,** 1660 (1971).
9. A. I. Ekimov, A. A. Onushchenko, A. G. Plyukhin and Al. L. Efros, Sov. Phys. JETP **88,** 891 (1985).
10. Al. L. Efros and A. V. Rodina, Solid State Commun. **72,** 645 (1989).
11. G. B. Grigoryan, E. M. Kazaryan, Al. L. Efros, and T. V. Yazeva, Sov. Phys. Solid State **32,** 1031 (1990).
12. J. B. Xia, Phys. Rev. B **40,** 8500 (1989).
13. A. I. Ekimov, Phys. Scr. **T39,** 217 (1991).

14. D. I. Chepic, Al. L. Efros, A. I. Ekimov, M. G. Ivanov, V. A. Kharchenko, I. A. Kudryavtsev, and T. V. Yazeva, J. Lumin. **47,** 113 (1990).
15. R. L. Aggarwal, in *Semiconductors and Semimetals*, R. K. Willardson and A. C. Beer, eds. (Academic, New York, 1972), Vol. 9, p. 151.
16. V. I. Sheka and D. I. Sheka, Sov. Phys. JETP **24,** 975 (1967).
17. G. B. Grigoryan, A. V. Rodina, and Al. L. Efros, Sov. Phys. Solid State **32,** 2037 (1990).
18. C. Hermann and C. Weisbuch, in *Optical Orientation*, F. Meier and B. P. Zakharchenya, eds. (Elsevier, Amsterdam, 1984), p. 443.
19. D. W. Hall and N. F. Borrelli, J. Opt. Soc. Am. B **5,** 1650 (1988).
20. N. Peyghambarian, B. Fluegel, D. Hulin, A. Migus, M. Joffre, A. Antonetti, S. W. Koch, and M. Lindberg, IEEE J. Quantum Electron. **25,** 2516 (1989).
21. M. G. Bawendi, W. L. Wilson, L. Rothberg, P. J. Carroll, T. M. Jedju, M. L. Steigerwald, and L. E. Brus, Phys. Rev. Lett. **65,** 1623 (1990).
22. M. C. Klein, F. Hache, D. Ricard, and C. Flytzanis, Phys. Rev. B **42,** 11123 (1990).
23. F. Hache, M. C. Klein, D. Ricard, and C. Flytzanis, J. Opt. Soc. Am. B **8,** 1802 (1991).
24. Al. L. Efros, A. I. Ekimov, F. Kozlowski, V. Petrova-Koch, H. Schmidbaur, and S. Shumilov, Solid State Commun. **78,** 853 (1991).